Advances in Applied Ceramics, Volume 117, 2018, Issue 5, pp. 303-311
DOI:10.1080/17436753.2017.1410941

Environmental blue $CoAl_2O_4$ pigment co-doped by Zn^{2+} and Mg^{2+}: synthesis, structure and optical properties

PENG Xiaojin[1, 2, 3], CHENG Jinshu[1, 3], YUAN Jian[1, 3], JIN Na[1], KANG Junfeng[1, 3], HOU Yansheng[1, 3], ZHANG Qi[3, 4, 5*]

[1]State Key Laboratory of Silicate Materials for Architectures, Wuhan University of Technology, Wuhan, 430070, Hubei, China

[2]CSIRO, Manufacturing, Clayton, VIC 3168, Australia.

[3]Glass and Technology Research Institute of Shahe, Shahe, 054100, Hebei, China

[4]State Key Laboratory of Advanced Technology for Materials Synthesis and Processing, Wuhan University of Technology, Wuhan 430070, Hubei, China

[5]School of Aerospace, Transportation and Manufacturing, Cranfield University, Cranfield, Bedfordshire, MK430AL, UK

Abstract: Nano-sized blue solid solutions $Zn_xMg_{0.5-x}Co_{0.5}Al_2O_4$ (x = 0 ~ 0.5) have been synthesized by the Pechini method. Single-phase $Zn_xMg_{0.5-x}Co_{0.5}Al_2O_4$ with crystallite size of ~40 nm was identified by XRD measurement. The TG-DSC results indicated that the phase formation temperature of $Zn_xMg_{0.5-x}Co_{0.5}Al_2O_4$ increased with the substitution of $Zn^{2+}/Mg^{2+} \rightarrow Co^{2+}$ proceeding. The UV-vis spectra illustrated that the $Zn_{0.3}Mg_{0.2}Co_{0.5}Al_2O_4$ pigment displayed the more intensive blue color with the strongest absorbance appearing within the visible region. The FT-IR spectra suggested that the inversion degree of $Zn_xMg_{0.5-x}Co_{0.5}Al_2O_4$ pigment reduces with the

* Corresponding author. Tel.: 44 (0) 1234 750111; Fax: 44 (0) 1234 751346
E-mail address: Q.Zhang@cranfield.ac.uk

increase of Zn^{2+} rather than Mg^{2+}, enabling to control the pigment color by tuning the Zn^{2+} content. The FESEM images showed the irregular shaped morphology of $Zn_xMg_{0.5-x}Co_{0.5}Al_2O_4$ crystal, different from cubic-like morphology of $CoAl_2O_4$ crystal. The XPS results illustrated that the inversion of pure $CoAl_2O_4$ pigment is larger than that of $Zn_{0.3}Mg_{0.2}Co_{0.5}Al_2O_4$. Both $Zn_{0.2}Mg_{0.3}Co_{0.5}Al_2O_4$ and $Zn_{0.3}Mg_{0.2}Co_{0.5}Al_2O_4$ were confirmed to enable the commercial potential in replacing the current $CoAl_2O_4$ pigments.

Keywords: Absorbance spectroscopy; Solid solutions; Citrate sol-gel method; Blue color; Inversion degree

1 Introduction

The natural and synthetic spinel-type (AB_2O_4) structure oxides, where divalent A and tervalent B cations occupy tetrahedral and octahedral crystallographic sites, respectively, have been widely used as ceramic pigments, magnetic materials and catalysts and so on. [1~4] Among them, Cobalt aluminate ($CoAl_2O_4$), known as Thenard's blue, is a typical blue inorganic pigment coupling with Co^{2+} ions in tetrahedral positions and Al^{3+} in octahedral positions. [5~8] This blue $CoAl_2O_4$ pigment has played a significant role in coloring our daily life, such as plastics coloring, paints, glasses, glazes and porcelain enamels. Except for its intensive blue color, the high resistance to acid and alkali and enhanced thermal stabilities are other prominent features of this inorganic blue pigment which should be highlighted. [9]

Recently, much researching enthusiasm has focused on how to obtain commercial $CoAl_2O_4$ pigment by optimizing the preparing process. The $CoAl_2O_4$ pigment is traditionally synthesized by solid-state reactions which involve the mechanical mixing of cobalt and aluminum oxides followed by calcinations at ~1300 ºC for over 2h as well as an extended grinding process. [3,10~12] However, this process requires a long-range diffusion of metal ions, which may result in a poor control of stoichiometry and inhomogeneous grains. [13] It is well known that

various wet-chemical methods have already shown advantages over solid-state reactions in the synthesis of nano-sized $CoAl_2O_4$ particles, including sol-gel method [14], hydrothermal treatment [15~16], Pechini method [17~18], reverse micro-emulsion method [19] and combustion method [20], and so on. These methods can effectively solve the above problems in solid-state process, so the Pechini method will be adopted in this paper.

Moreover, as the main contributor for generating blue color of $CoAl_2O_4$ pigment, the cobalt element has already aroused great issues of both toxicity and scarcity. The hazardous cobalt element is widely considered to have an environmental impact on the industrial manufacturing process. Also, being a rare natural resource, the use of cobalt element assuredly aggrandizes the production costs. In these respects, the most direct practice is to reduce the amount of Co^{2+} in $CoAl_2O_4$ spinel by adding some alternative elements, such as Zn^{2+} and/or Mg^{2+},. This procedure can not only reduce the utilization of expensive and toxic cobalt element but also produce commercial pigment with promoted performance. The improvement of structure and optical properties of $CoAl_2O_4$ pigments by Zn^{2+} and Mg^{2+} ions doping can be confirmed by the following efforts: $Zn_{1-x}Co_xAl_2O_4$ [8,17], $Co_xMg_{1-x}Al_2O_4$ [21], as well as $Zn_{2-x}Co_xSiO_4$ [22], $Co_{1-x}Zn_xCr_{2-y}Al_yO_4$ [7], $Mg_{2-x}Co_xAl_4Si_5O_{18}$ [23], and so on. The pigments of $Mg_xCo_yAl_2O_4$ type were

also proved to enable to present different colors, depending on particle shape and size, bulk density, and doping concentrations. Meanwhile, the pigments of $Zn_xCo_yAl_2O_4$ type exhibited the blue color ranging, markedly NIR solar reflectance and NIR reflective performance with Zn^{2+} ions replacing Co^{2+} ions in part. [7~8, 31] Nonetheless, there exists scarcely related literatures about the influence of co-doping Zn^{2+} and Mg^{2+} ions in structure and optical properties of $CoAl_2O_4$ blue pigments. To make aforesaid issue clearly, we performed the investigations on spinel-type nano-sized crystalline $Zn_xMg_{0.5-x}Co_{0.5}Al_2O_4$ pigment.

In this study, the precursor powders of crystalline $Zn_xMg_{0.5-x}Co_{0.5}Al_2O_4$ (x=0, 0.1, 0.2, 0.3, 0.4, 0.5) were synthesized by the Pechini method and then calcined at 250 ºC for 2h to form the final nano-sized pigments. The influences of relative content of Zn^{2+} and Mg^{2+} on morphological feature and crystal structure of particles as well as structural and optical properties of the pigments were investigated in detail. The optimal samples were selected for potential commercial applications.

2 Experimental

2.1 Materials and synthesis

All the raw chemical reagents are analytical pure grade: zinc acetate dehydrate ($C_4H_6ZnO_4 \cdot 2H_2O$), magnesium acetate tetrahydrate ($C_4H_6MgO_4 \cdot 4H_2O$), cobalt nitrate ($Co(NO_3)_2 \cdot 6H_2O$), aluminum nitrate ($Al(NO_3)_3 \cdot 9H_2O$), citric acid (CA) and ethyl alcohol (EA), which were all provided by Sinopharm Chemical Reagent Co., Ltd, Shanghai, China. The Standard commercial $CoAl_2O_4$ blue pigment (BU612) was used as a reference pigment, which was purchased from Nanjing Pigments Tech. Co., Ltd.

The polymeric precursor method was selected to synthesize polycationic powders. This method is based on three parts: the cations chelation by citric acid (CA) in an aqueous solution, the polyesterification between carboxylic groups of CA and hydroxyl groups of EA forming polycationic resin when heating and stirring.[4, 24~25] In our experiment, 0.015 mol $Co(NO_3)_2 \cdot 6H_2O$ and 0.06 mol $Al(NO_3)_3 \cdot 9H_2O$ were firstly dissolved in 100 ml distilled water under constant magnetic stirring at 60 ºC for 30 min., following by the addition of 0.27 mol CA and the solution was stirred for another 30 min. at 60 ºC. Meanwhile, 0.03x (x=0, 0.1, 0.2, 0.3, 0.4 and 0.5) mol $C_4H_6ZnO_4 \cdot 2H_2O$ and 0.03(0.5-x) mol $C_4H_6MgO_4 \cdot 4H_2O$ were also dissolved in EA completely at 60 ºC for 1h. These samples are named as ZM2~7, while ZM1 is the pure $CoAl_2O_4$ crystal without any Zn^{2+} and Mg^{2+} doping. The molar ratios of metal/(CA) and (EA/CA) were set as 1:3 and 2:3, separately. Subsequently, the

aforesaid EA was added into CA solutions and kept further stirring for 2 h at 80 ºC. During the process of removing excess water through continuous heating, the purple solution became more and more viscous until a xerogel formed. [4] Ultimately, the xerogel was underwent a preliminary heat treatment at 250 ºC for 2 h in air, to remove most of organic solvents and water. [8] After that, the dry xerogel was milled into a fine powder followed by a calcination at 1000 ºC for 2h in air. The flow chart of the whole preparing process is exhibited in Fig. 1.

2.2 Measurements and characterization

The thermal behavior of pigment precursors was examined by a thermogravimetry and differential scanning calorimetry analyzer (TG-DSC, Netzsch STA 449 F3 instrument). Alumina was used as a reference material. The TG-DSC curves were recorded at a heating rate of 10 ℃·min^{-1} over the temperature range of 25 ~ 1000 ºC, inflowing air rate of 20 mL·min^{-1}. The crystal structures and phase composition of sintered pigments were characterized by X-ray diffraction (XRD, D/MAX-UItimaIV, Rigaku). The Cu *Kα* radiation (λ = 0.15405 μm) was used at 40 KV and 40 mA. The diffraction patterns were recorded with 2θ = 10° ~ 70°. UV-vis diffuse reflectance spectra (UV-vis DRS) were signed in the absorbance mode at room temperature in the range of 300 ~ 800 nm on Lambda 750 S apparatus, using $BaSO_4$ as a reference material. Fourier transform infrared (FT-IR) spectra were recorded on Therno

Nicolet NEXUS equipment with a Nicolet 750 spectrometer. The commission internationale de L'eclairage (CIE-$L^*a^*b^*$) values were measured by a spectrocolorimeter (CM-2600d), in which L^* is the lightness axis [black (0), white (100)], a^* is the green (−) to red (+) axis, and b^* is the blue (−) to yellow (+) axis. The particle size and morphology of calcined pigment were observed by a field emission scanning electron microscope (FE-SEM, Zeiss Ultra Plus) instrument. The X-ray photoelectron spectra (XPS) were measured by ESCALAB 250Xi spectrometer with mono-chromatized Al Kα X-ray radiation in ultrahigh vacuum ($<10^{-7}$ Pa). The binding energies were calibrated by taking C1s peak (284.6 eV) of adventitious carbon as a reference. The peaks were deconvoluted after background subtraction, using a mixed Gaussian-Lorentzian function. Fractional atomic concentrations of the elements were calculated using empirically derived atomic sensitivity factors. [26]

3 Results and discussion

3.1 Thermal analysis

The TG-DSC curves of two typical precursors ($CoAl_2O_4$ and $Zn_{0.3}Mg_{0.2}Co_{0.5}Al_2O_4$) are shown in Fig. 2, which indicates that the whole phase formation process can be divided into three steps. The first

endothermic peak at ~80 ºC and the adjacent weak endothermic peak at ~130 ºC are observed due to the elimination of the co-ordination water and the decomposition of remaining nitrates and acetates in samples, respectively, coupling with a mass loss of ~10% in the first range of 0 ~ 200 ºC [14, 21]. The DSC curves from 200 ºC to 700 ºC exhibit two obvious exothermic peaks, where the exothermic peak at ~400 ºC is attributed to the burning of organics [21] while the exothermic peak at ~500 ºC corresponds to the formation of $CoAl_2O_4$ crystal. [2] There is also a more distinct mass loss of about 60% at temperature higher than 200 ºC. The last step is the formation of $Zn_{0.3}Mg_{0.2}Co_{0.5}Al_2O_4$ compound with a feeble exothermic peak at ~700 ºC and no evident mass loss was detected on TG curve (see Fig. 2a), which is in accordance with the findings by Zayat et al and Kurajica et al [6, 14].

Although the main exothermic and endothermic peaks of both $CoAl_2O_4$ and $Zn_{0.3}Mg_{0.2}Co_{0.5}Al_2O_4$ exhibited in Fig. 2 are very alike at the temperature below 450 ºC, there still exist some minor differences between two samples at higher temperature. Obviously, after adding Zn^{2+} and Mg^{2+} into $CoAl_2O_4$, the strongest crystalline peak position was shifted from ~446 ºC of $CoAl_2O_4$ in Fig. 2 (a) to ~478 ºC of $Zn_{0.3}Mg_{0.2}Co_{0.5}Al_2O_4$ in Fig. 2 (b) and the intensity of the exothermic peak was enhanced as well. Zn^{2+} and Mg^{2+} have approximate ionic radius to Co^{2+} (0.074 nm for Zn^{2+}, 0.072 nm for Mg^{2+} and 0.0745 nm for Co^{2+},

respectively), which facilitates the substitution of the Co^{2+} by Zn^{2+} and Mg^{2+} during the formation process of $CoAl_2O_4$ spinel crystallite. The small difference in ionic radii could still lead to the deformation of the unit cell and the ions transferred strenuously, which exhibits a higher crystallizing temperature and a stronger exothermic intensity in DSC curves as shown in Fig. 2 (b). Moreover, the DSC and TG curves in Fig. 2 illustrate that no further chemical or physical reactions occurred at 700 ºC above, implying the end of the redox processes at 700 ºC.

3.2 Crystal formation and structure analysis

The XRD patterns of pigments, $CoAl_2O_4$ and $Zn_xMg_{0.5-x}Co_{0.5}Al_2O_4$ (x=0.1, 0.2, 0.3 and 0.4) synthesized at 1000℃ for 2h, are illustrated in Fig. 3. The observed diffraction peaks in the pattern (a) are in good agreement with those of standard $CoAl_2O_4$ spinel (JCPDS card NO.: 44-0160). No traces of other impurity phases can be observed. The typical diffraction peaks in XRD patterns of (b) ~ (e) for $Zn_xMg_{0.5-x}Co_{0.5}Al_2O_4$ (x=0.1~0.4) can be identified as the standard spinel crystals, $CoAl_2O_4$ spinel (JCPDS card NO.: 44-0160), $ZnAl_2O_4$ spinel (JCPDS card NO.: 05-0669) and $MgAl_2O_4$ spinel (JCPDS card NO.: 21-1152). The phase analysis manifests that the main phases of $Zn_xMg_{0.5-x}Co_{0.5}Al_2O_4$ powders, cubic spinel structure and space group Fd3m, exist in a form of solid-solution.

Based on XRD patterns (b) ~ (e) of the $Zn_xMg_{0.5-x}Co_{0.5}Al_2O_4$ samples, the effect of varying *x* values on the crystallization behavior of $CoAl_2O_4$ spinel crystal was studied. With the increase of *x* value, both [3 1 1] and [3 3 1] peak intensities increase initially but decrease afterwards, though both peak intensities were still stronger than those of pure $CoAl_2O_4$ crystal phase. Furthermore, the relative intensities of the [2 2 0] and [3 1 1] peaks enhance and reach maxima when x reaches 0.4 ($Zn_{0.4}Mg_{0.1}Co_{0.5}Al_2O_4$), which is also coupled with a small shift of [3 1 1] from 36.78° to 36.84°. These peak intensity and position changes were associated with the small change of lattice deformation which was caused by the co-substitution of Zn^{2+} and Mg^{2+}. [7]

The average crystallite size (D_{hkl}) of the samples was calculated by Debye-Scherrer formula, [7, 27]

$$D_{hkl} = \frac{K \cdot \lambda}{\beta \cdot \cos\theta}$$

where β is the breadth of the observed diffraction line at its half-intensity maximum; K the shape constant and usually a value of about 0.9; λ the wavelength of the Cu=K_α radiation (1.5406 Å); θ the diffraction angle. The average D_{hkl} of the samples were listed in Table 1, which were found to be in the nano-sized range of 39-43 nm. Because citric acid was introduced into this mixture, the organic ligand capped the nanocrystals surface, thus inhibiting the growth of the particles. [4] However,

$Zn_{0.3}Mg_{0.2}Co_{0.5}Al_2O_4$ sample possesses the minimum crystallite size 39 nm among all samples with various molar ratios of Zn^{2+} and Mg^{2+}, as seen in Table 1.

3.3 XPS spectra analyses

In our experiment, the chemical states of the elements on the surface region of as-synthesized pigments $CoAl_2O_4$ and $Zn_{0.3}Mg_{0.2}Co_{0.5}Al_2O_4$ are characterized by X-ray photoelectron spectroscopy (XPS) and the results are shown in Fig. 4. The spectra indicate that no other elements were detected except for the original components and contaminated carbon. The C 1s peak at about 284.6 eV was used as a reference, while O 1s peak shows asymmetric and fixed on 531.5 ± 0.2 eV which is in accordance with that of O 1s in bulk $CoAl_2O_4$ reported by Patterson et al.. [41]

The coordination change of Co^{2+} and Al^{3+} in the surface region of pigments doped by Zn^{2+} and Mg^{3+} can be observed by the Co 2p and Al 2p peaks in Fig. 7b and d. The Co $2p_{3/2}$ core level peak is fixed at 781.9 eV with the broad satellite around 786.6 eV after deconvolution and that of Co $2p_{1/2}$ is 797.2 eV with the broad satellite about 803.7 eV, respectively, which are similar to the results reported by Zsoldos et al. [42] and Chung et al.. [43] All the Co 2p spectra are relatively broad and asymmetric, indicating that the Co^{2+} occupies both octahedral and tetrahedral coordination positions in as-synthesized samples. In addition,

the main peaks at lower binding energy (781.9 eV and 797.2 eV) can be ascribed to Co^{2+} ions placed at the octahedral sites, while the broad peak at higher binding energy (786.6 eV and 803.7 eV) are attributed to Co^{2+} fixed on tetrahedral positions. Similarly, the Al 2p peaks are focused on around 74.5 eV and 74.0 eV after deconvolution, which are due to octahedral Al^{3+} ions and tetrahedral Al^{3+} ions, separately.

Furthermore, the tetrahedral Co^{2+} ions and tetrahedral Al^{3+} ions are dominant in all the studied samples. On the basis of above discussion, the as-synthesized $CoAl_2O_4$ and $Zn_{0.3}Mg_{0.2}Co_{0.5}Al_2O_4$ pigments can be treated as a partially inversed spinel-structure. The inversion parameter k can be estimated according to the area ratio of the two peaks, which correspond to the Co^{2+} and Al^{3+} on octahedral and tetrahedral sites, respectively. In our experiment, the k value for $CoAl_2O_4$ and $Zn_{0.3}Mg_{0.2}Co_{0.5}Al_2O_4$ pigments are 0.20 and 0.01, respectively. The result indicates that the inversion degree of pure $CoAl_2O_4$ pigment is larger than that of $Zn_{0.3}Mg_{0.2}Co_{0.5}Al_2O_4$ pigment. Also, the inverse degree are related to the particle size, and the increasing k will decrease the small particle size, fitting with the reports by Duan et al.. [2]

3.4 Surface morphology analyses

The surface morphology of the synthesized $CoAl_2O_4$ and $Zn_{0.3}Mg_{0.2}Co_{0.5}Al_2O_4$ pigments was investigated by FE-SEM and the results were illustrated in Fig. 5. From the above images (a) ~ (d), it is

clearly shown that the particles of two samples have diverse surface morphologies with the particle size ranging from 30 nm to 100 nm. The cubic-like morphology was obviously observed in the case of $CoAl_2O_4$ powders, which is different from the irregular shaped morphology of $Zn_{0.3}Mg_{0.2}Co_{0.5}Al_2O_4$ powders. Besides, the addition of Zn^{2+} and Mg^{2+} would reduce the uniformity of particles of $CoAl_2O_4$ pigment. Additionally, the particles of $CoAl_2O_4$ sample tend to be more agglomerate than that of $Zn_{0.3}Mg_{0.2}Co_{0.5}Al_2O_4$ powders.

3.5 UV-vis spectra analyses

Fig. 6 illustrates the UV-vis absorbance spectra of (a) $CoAl_2O_4$;$Zn_xMg_{0.5-x}Co_{0.5}Al_2O_4$ system: (b) x=0; (c) x=0.2; (d) x=0.3; (e) x=0.5 calcined at 1000℃ for 2h and (f) BU612 commercial blue $CoAl_2O_4$ pigment. All the spectra manifest a common feature: a strong and triple absorption band can be observed from 540 nm to 650 nm, which is within the visible region (400 nm ~ 780 nm). According to Tanabe Sugano energy level diagrams, the Co^{2+} in $[CoO_4]$ with d^7 configuration, ^4F ground state term splits into three terms $^4A_2$, $^4T_2$ and $^4T_1(F)$ as well as ^4P excited state term changes to $^4T_1(P)$. Thereby, the three spin allowed transitions are as follows: v_1: $^4A_2(F) \rightarrow {}^4T_2(F)$; v_2: $^4A_2(F) \rightarrow {}^4T_1(F)$ and v_3: $^4A_2(F) \rightarrow {}^4T_1(P)$, with the first two bands in the IR region while the third band in the visible region.[28~29] The third spin allowed $^4A_2(F) \rightarrow {}^4T_1(P)$ transition of Co^{2+} ions in tetrahedral sites divides into three secondary

bands (see in Fig. 4) ~550 nm (peak I), ~580 nm (peak II) and ~620 nm (peak III), respectively.

As for many inorganic Co-based blue pigments with a spinel structure, the Co^{2+} ions located on tetrahedral sites play a crucial role in the pigments expressing blue color [8, 30]. To be more specific, spin-allowed $^4A_2(F) \rightarrow {}^4T_1(P)$ transition of the Co^{2+} ions in tetrahedral sites is corresponding to the absorption of the colors, such as, yellow, orange and red, thus the reflectance occurs in the complementary colors, such as, violet, blue and cyan, but centered in the blue color.[31] Furthermore, the absorption peak at ~481nm (peak IV) is influenced by the spin forbidden $^4A_2(F) \rightarrow {}^2T(G)$ transition of Co^{2+} ions in octahedral positions of spinel structure, while this new band results in green color.[2, 14, 32] The same band generated by octahedrally coordinated Co^{2+} has also been reported by other authors.[33~34] Other weak bands marked at ~400 nm (peak V) are also associated with the spin forbidden transition presented by Zayat et al. [14]

In our present work, the different substituting effect of Zn^{2+} and Mg^{2+} on exhibiting the blue color of $CoAl_2O_4$ pigment can be obtained according to the degree of the third spin allowed $^4A_2(F) \rightarrow {}^2T(G)$ transition as well as absorbance intensity of three peaks (I, II and III) in UV-vis absorbance curves as shown in Fig. 6. With the x value increasing, the absorbance intensity of three peaks (I, II and III) of $Zn_xMg_{0.5-}$

$_xCo_{0.5}Al_2O_4$ system pigments climbed up primarily, reached the maximum at x = 0.3 and then declined gradually. Namely, the Zn^{2+} plays a more important role in promoting the blue color of $CoAl_2O_4$ pigment than Mg^{2+} when x value is less than 0.3 but that would be completely opposite when x value is larger than 0.3. According to the decisive effect of the triplet band absorption pattern (peaks I, II and III) on the blue color generation, the $Zn_{0.3}Mg_{0.2}Co_{0.5}Al_2O_4$ pigment shows the most intensive blue color which is also stronger than that of commercial $CoAl_2O_4$ blue pigment (BU612). These findings can also be confirmed by the related UV-vis results in Fig. 6 and the pictures of pigments in Fig. 8. In other words, from the view of developing environmental pigment, the $Zn_{0.3}Mg_{0.2}Co_{0.5}Al_2O_4$ pigments with enhanced blue color can be selected as an alternative for current commercial $CoAl_2O_4$ pigment due to lowering the usage of Co element.

3.6 FT-IR spectra analyses

FT-IR analysis was conducted to characterize the resulting pigments subjected to the heat treatment at 1000℃ for 2h and the results are presented in Fig. 7. The spectra shows two obvious absorption bands at around 662-681 $cm^{-1}$and 555-560 cm^{-1} and a weak absorption band at about 507-509 cm^{-1}, associated with the vibrations of metal-oxygen, aluminum-oxygen and metal-oxygen-aluminum, respectively. [4] The

changes of absorption intensity with x ranging from 0 to 0.5 are the most apparent for the bands at the highest wave numbers. The band centered at ~681 cm^{-1} dominates for $Mg_{0.5}Co_{0.5}Al_2O_4$ pigments, which is different from other four samples. Dominance shifts to the two bands centered at ~ 673 cm^{-1} and ~560 cm^{-1} with the increase of Zn^{2+} ions in the spinel structure. All the three bands at ~ 673 cm^{-1}, ~560 cm^{-1} and ~507 cm^{-1} of $Zn_{0.2}Mg_{0.3}Co_{0.5}Al_2O_4$ pigments show the strongest absorption intensity among all the samples. What's more, the absorption intensity of these three bands of $Zn_{0.2}Mg_{0.3}Co_{0.5}Al_2O_4$ is much higher than that of ether synthetic $CoAl_2O_4$ or commercial CoAl2O4 pigment.

In literatures, the spinel crystals should exhibit three normal vibrational modes in the middle IR region, whereas various factors can lead to an increase in the number of IR modes. [35~36] Wang et al. [37] and Chapskaya et al. [38] have found that for normal $CoAl_2O_4$ spinel the vibrations occur at ~666 cm^{-1}, ~554cm^{-1} and ~504 cm^{-1}, comparing to these characteristic bands of inverse spinel occurred at ~626 cm^{-1}, ~559cm^{-1} and ~480 cm^{-1}. The absorption band at ~666 cm^{-1} is generally assigned to the Al-O stretching vibration of the [AlO_6] octahedral in normal spinel, while the absorption band at ~ 626 cm^{-1} points outs the tetrahedrally coordinated aluminum, which exists in inverse spinel. The bands at 555-560 cm^{-1} are identified as (CoO_4), (ZnO_4) and (MgO_4) vibrations which are in agreement with the findings by Chen et al [39]

and Ahmed et al. [21] What's more, Meyers et al [40] ascribed 470-900 cm^{-1} and 340-550 cm^{-1} to the Al-O and Co-O stretching frequencies, respectively, whereas the Al-O-Co frequencies were noted in the 450-800 cm^{-1} region.

The band at the highest wave number intensively concentrates at ~ 673 cm^{-1}, which could be related to the [AlO_4] as well as inverse spinel. The different relative intensities of absorption bands at ~673 cm^{-1} decrease with the increase of Zn^{2+} ions content, indicating that Zn^{2+} shows a more obvious inhibiting effect in $CoAl_2O_4$ spinel being inversed than Mg^{2+}. However, more work needs to be done to reveal the inner relation between Zn^{2+} & Mg^{2+} and the inverse degree of $CoAl_2O_4$ spinel.

3.7 CIE-$L^*a^*b^*$ color measurement

The color changes of Co-based pigments were investigated and the results are shown in Fig. 8. It's obvious that the blue color of the $CoAl_2O_4$ pigment is darker than that of $Zn_xMg_{0.5-x}Co_{0.5}Al_2O_4$ pigments, in accordance with the decreasing L^* values in Table 1. Besides, with the increase of *x* value from 0 to 0.5, the colors of $Zn_xMg_{0.5-x}Co_{0.5}Al_2O_4$ pigments are hardly distinguished by human eye, whereas the weakened difference can be confirmed by changes of L^* and b^*. When the ratio of Zn^{2+}/Mg^{2+} was 3:2 or 4:1, the more negative b* values of pigments were measured, -28.27 and -27.98, respectively, which are more negative than the rest of samples. Moreover, for the extreme composition, the changes

of b^* of $Zn_{0.5}Co_{0.5}Al_2O_4$ (x = 0.5) is negligible comparing with $Mg_{0.5}Co_{0.5}Al_2O_4$ (x = 0), whereas the L^* values increase largely from 33.26 to 44.88, indicating that the substituting Zn^{2+} ions are more likely to the lighter pigments. Hence, taking the application of pigment into consideration, the $Zn_{0.3}Mg_{0.2}Co_{0.5}Al_2O_4$ and $Zn_{0.2}Mg_{0.3}Co_{0.5}Al_2O_4$ pigments can be used as an environmental blue coating pigment for replacing the current $CoAl_2O_4$ pigment.

4 Conclusions

In conclusion, blue pigments $CoAl_2O_4$ and $Zn_xMg_{0.5-x}Co_{0.5}Al_2O_4$ (x=0, 0.1, 0.2, 0.3, 0.4, 0.5) solid-solution nanocrystals have been successfully synthesized by Pechini method. The effects of Zn^{2+} and Mg^{2+} enrichment on the crystal formation, morphological and optical properties were investigated. TG-DSC and XRD results show that the substitution of Zn^{2+}/Mg^{2+} to Co^{2+} can increase the phase formation temperature of $Zn_xMg_{0.5-x}Co_{0.5}Al_2O_4$ solid-solution typed crystals with a particle size of 39-43 nm. According to the UV-vis results, the triple absorption bands from 540 nm to 650 nm are related to the spin-allowed [$^4A_2(F)\rightarrow{}^4T_1(P)$] transition of tetrahedral Co^{2+} in spinel structure. Besides, the $Zn_{0.3}Mg_{0.2}Co_{0.5}Al_2O_4$ pigment has stronger absorbance than other Zn^{2+}/Mg^{2+} doping pigments within the visible region, which shows the more intensive blue color. FT-IR spectra revealed that the increase of

substituting Zn^{2+} ions content can reduce the inversion degree of $CoAl_2O_4$ spinel structure, which is more obvious than that of Mg^{2+}. Moreover, the difference of blue color of as-synthesized pigments can hardly be distinguished by human eye, but both $Zn_{0.2}Mg_{0.3}Co_{0.5}Al_2O_4$ and $Zn_{0.3}Mg_{0.2}Co_{0.5}Al_2O_4$ show the potential commercial application. FESEM images indicate the different surface morphology of $CoAl_2O_4$ and $Zn_xMg_{0.5-x}Co_{0.5}Al_2O_4$ pigments, cubic-like and irregular shape, respectively. XPS results show that the Co^{2+} and Al^{3+} ions occupy both the tetrahedral and octahedral sites in cubic spinel structure. The inversion degree of pure $CoAl_2O_4$ pigment is larger than that of $Zn_{0.3}Mg_{0.2}Co_{0.5}Al_2O_4$ pigment.

5 Acknowledgements

Authors are grateful to the Chinese Government's Fundamental Research Funds for the Central Universities (2016-JL-002) and Glass and Technology Research Institute of Shahe, China.

References

[1] Gul IH, Maqsood A, Naeem M, et al. Optical, magnetic and electrical investigation of cobalt ferrite nanoparticles synthesized by co-precipitation route. J Alloys Compd 2010; 506: 201-6.

[2] Duan X, Pan M, Yu F, et al. Synthesis, structure and optical properties of $CoAl_2O_4$, spinel nanocrystals. J Alloys Compd 2011; 509:1079-83.

[3] Yu F, Yang J, Ma J, et al. Preparation of nanosized $CoAl_2O_4$, powders by sol–gel and sol–gel-hydrothermal methods. J Alloys Compd 2009; 468: 443-6.

[4] Salavati-Niasari M, Farhadi-Khouzani M, Davar F. Bright blue pigment $CoAl_2O_4$ nanocrystals prepared by modified sol–gel method. J Sol-Gel Sci Techn 2009; 52: 321-7.

[5] Buxbaum G. Industrial Inorganic Pigments. 1st ed. Germany: Weinheim; 1993.

[6] Kurajica S, Popović J, Tkalčec E, et al. The effect of annealing temperature on the structure and optical properties of sol-gel derived nanocrystalline cobalt aluminate spinel. Mater Chem Phys 2012; 135: 587-93.

[7] Hedayati HR, Sabbagh Alvanib AA, Sameie H, et al. Synthesis and characterization of $Co_{1-x}Zn_xCr_{2-y}Al_yO_4$ as a near-infrared reflective color tunable nano-pigment. Dyes Digments 2015; 113: 588-95.

[8] Souza LKCD, Zamian JR, Filho GNDR, et al. Blue pigments based on $Co_xZn_{1-x}Al_2O_4$ spinels synthesized by the polymeric precursor method. Dyes Pigments 2009; 81: 187-92.

[9] Li W, Li J, Guo J. Synthesis and characterization of nanocrystalline $CoAl_2O_4$ spinel powder by low temperature combustion. J Eur Ceram Soc 2003; 23: 2289–95.

[10] Peymannia M, Soleimani-Gorgani A, Ghahari M, et al. The effect of different dispersants on the physical properties of nano $CoAl_2O_4$ ceramic ink-jet ink. Ceram Int, 2015; 41: 9115-21.

[11] Burdett J K, Price GD, Price S L. Role of the crystal-field theory in determining the structures of spinels. J Am Chem Soc 1982; 104: 238-44.

[12] Wang C, Liu S, Liu L, et al. Synthesis of cobalt–aluminate spinels via glycine chelated precursors. Mater Chem Phys 2006; 96: 361-70.

[13] Meyer F, Hempelmann R, Mathur S, et al. Microemulsion mediated sol-gel synthesis of nano-scaled MAl_2O_4 (M=Co, Ni, Cu) spinels from single-source heterobimetallic alkoxide precursors. J Mater Chem 1999; 9: 1755-63.

[14] Zayat M, Levy D. Blue $CoAl_2O_4$ particles prepared by the Sol−Gel and citrate-gel methods. Chem Mater 2000; 12: 2763-69.

[15] Chen ZZ, Shi EW, Li WJ, et al. Preparation of nanosized cobalt aluminate powders by a hydrothermal method. Mater Sci Eng B 2004; 107: 217-23.

[16] Gaudon M, Apheceixborde A, Ménétrier M, et al. Synthesis temperature effect on the structural features and optical absorption of $Zn_{1-x}Co_xAl_2O_4$ oxides. Inorg Chem 2009; 48: 9085-91.

[17] Gama L, Ribeiro MA, Barros BS, et al. Synthesis and characterization of the $NiAl_2O_4$, $CoAl_2O_4$, and $ZnAl_2O_4$ spinels by the polymeric precursors method. J Alloys Compd 2009; 483: 453-55.

[18] Lu J, Minami K, Takami S, et al. Rapid and continuous synthesis of cobalt aluminate nanoparticles under subcritical hydrothermal conditions with in-situ, surface modification. Chem Eng Sci 2013; 85: 50-4.

[19] Chandradass J, Balasubramanian M, Kim KH. Size effect on the magnetic property of $CoAl_2O_4$ nanopowders prepared by reverse micelle processing. J Alloys Compd 2010; 506: 395-99.

[20] Salem S, Jazayeri SH, Bondioli F, et al. Co Al_2O_4 nano pigment obtained by combustion synthesis. Int J Appl Ceram Tec 2011; 9: 968-78.

[21] Ahmed IS, Shama SA, Dessouki HA, et al. Low temperature combustion synthesis of $Co_xMg_{1-x}Al_2O_4$ nano pigments using oxalyldihydrazide as a fuel. Mater Chem Phys 2011; 125: 326-33.

[22] Ahamdane H, El MA, Raghni I, et al. Elaboration and characterization of Co-Zn_2SiO_4 pigments. Adv App Microbiol 2013; 03: 91-00.

[23] Ianosev S, Lazău I, Păcurariu C, Avramescu A. Cordierite ($2MgO_2 \cdot Al2O_3 \cdot 5SiO_2$) synthesis by unconventional methods. Process Appl Ceram 2008; 2: 39-4.

[24] Bouquet V, Bernardi MIB, Zanetti SM, et al. Epitaxially grown $LiNbO_3$ thin films by polymeric precursor method. J Mater Res 2000; 15: 2446-53.

[25] Lin J, Yu M, Lin C, Liu X. Multiform oxide optical materials via the versatile Pechini-type sol-gel process: synthesis and characteristics. J Phys Chem C 2007;111: 5835-45.

[26] Wagner CD, Davis LE, Zeller MV, et al. Empirical atomic sensitivity factors for quantitative analysis by electron spectroscopy for chemical analysis. Surf Interface Anal 1981; 3: 211-25.

[27] Jenkins R, Snyder RL. Diffraction theory: Introduction to X-ray powder diffractometry. New York: Wiley; 1996.

[28] Llusar M, Fores A, Badenes JA, Calbo J, Tena MA, Monros G. Colour analysis ofsome colbat-based blue pigments. J Eur Ceram Soc 2001; 21: 1121-30.

[29] Huheey JE, Keiter EA, Keiter RL. Inorganic chemistry: principles of structure and reactivity. 4th ed. New York: Harper Collins; 1993.

[30] Mason RK. Use of cobalt colors in glazes. Am Ceram Soc Bull 1961; 40: 5-6.

[31] Ianoş R, Lazău R, Barvinschi P. Synthesis of $Mg_{1-x}Co_xAl_2O_4$ blue pigments via combustion route. Adv Powder Techno 201; 22: 396-400.

[32] Stangar UL, Orel B, Krajnc M. Preparation and spectroscopic characterization of blue $CoAl_2O_4$ coatings. J Sol-Gel Sci Techn 2003; 26: 771-75.

[33] Cava S, Tebcherani SM, Pianaro SA, et al. Structural and spectroscopic analysis of γ-Al_2O_3 to α-Al_2O_3-$CoAl_2O_4$ phase transition. Mater Chem Phys 2006; 97: 102-08.

[34] Matteucci F, Cruciani G, Dondi M, et al. Crystal structure, optical properties and colouring performance of karrooite $MgTi_2O_5$ ceramic pigments. J Solid State Chem 2007; 180: 3196-10.

[35] Julien CM, Gendron F, Amdouni A, et al. Lattice vibrations of materials for lithium rechargeable batteries. VI: Ordered spinels. Mater Sci and Eng B 2006; 130: 41-48.

[36] Kringe C, Oft B, Schellenschläger V, et al. Infrared spectroscopic studies on spinel-type chromium indium sulfide solid solutions. J of Mol Struct 2001; 596: 25-32.

[37] Wang C, Liu S, Liu L, et al. Synthesis of cobalt–aluminate spinels via glycine chelated precursors. Mater Chem Phys 2006; 96: 361-370.

[38] Chapskaya AY, Radishevskaya NI, Kasatskii NG, et al. The effect of composition and synthesis conditions on the structure of cobalt-bearing pigments of the spinel type. Glass Ceram 2005; 62: 388-390.

[39] Chen Z, Shi E, Li W, Aheng Y, Zhong W. Hydrothermal synthesis and optical property of nano-sized $CoAl_2O_4$ pigment. Mater Lett 2002; 55: 281-84.

[40] Meyer F, Hempelmann R, Mathur S, Veith M. Microemulsion mediated sol–gel synthesis of nano-scaled MAl_2O_4 (M=Co, Ni, Cu) spinels from single-source heterobimetallic alkoxide precursors. J Mater Chem 1999; 9: 1755-63.

[41] Patterson TA, Carver JC, Leyden DE, et al. A surface study of cobalt-molybdena-alumina catalysts using X-ray photoelectron spectroscopy. J Phys Chem 1976; 80: 1700-08.

[42] Zsoldos Z, Guczi L. Structure and catalytic activity of alumina supported platinum-cobalt bimetallic catalysts. 3. Effect of treatment on the interface layer. J Phys Chem 1992; 96: 9393-00.

[43] Chung KS, Massoth FE. Studies on molybdena-alumina catalysts: VII. Effect of cobalt on catalyst states and reducibility. J Catal 1980; 64: 320-31.

Figure captions

Fig. 1 The flow chart of preparing process for ZnxMg0.5-xCo0.5Al2O4 powders

Fig. 2 TG-DSC curves of pigment precursors: (a) $CoAl_2O_4$ and (b) $Zn_{0.3}Mg_{0.2}Co_{0.5}Al_2O_4$ (ZM5) preliminarily heated at 250℃ for 2 h

Fig. 3 XRD patterns of pigments: (a) $CoAl_2O_4$ and $Zn_xMg_{0.5-x}Co_{0.5}Al_2O_4$ system: (b) x=0.1; (c) x=0.2; (d) x=0.3; (e) x=0.4

Fig. 4 XPS spectra of the as-synthesized $CoAl_2O_4$ and $Zn_{0.3}Mg_{0.2}Co_{0.5}Al_2O_4$ nano-sized crystal calcined at 1000 ℃ for 2h

Fig. 5 FESEM images of the (a) undispersed and (b) dispersed $CoAl_2O_4$ pigments; (c) undispersed and (d) dispersed $Zn_{0.3}Mg_{0.2}Co_{0.5}Al_2O_4$ pigments

Fig. 6 UV-vis absorbance spectra of pigments: (a) $CoAl_2O_4$ and $Zn_xMg_{0.5-x}Co_{0.5}Al_2O_4$ system: (b) x=0; (c) x=0.2; (d) x=0.3; (e) x=0.5; (f) commercial $CoAl_2O_4$ pigment (BU612).

Fig. 7 FT-IR spectra of (a) $CoAl_2O_4$ and $Zn_xMg_{0.5-x}Co_{0.5}Al_2O_4$: (b) x = 0; (c) x = 0.2; (d) x = 0.3; (e) x = 0.5 calcined at 1000℃ for 2h; (f) commercial $CoAl_2O_4$ pigment (BU612).

Fig. 8 Photographs of the (a) $CoAl_2O_4$ and $Zn_xMg_{1-x}Co_{0.5}Al_2O_4$: (b) x=0; (c) x=0.3; (d)x=0.4; (e) x=0.5 pigments; (f) commercial $CoAl_2O_4$ pigment (BU612).

Figures:

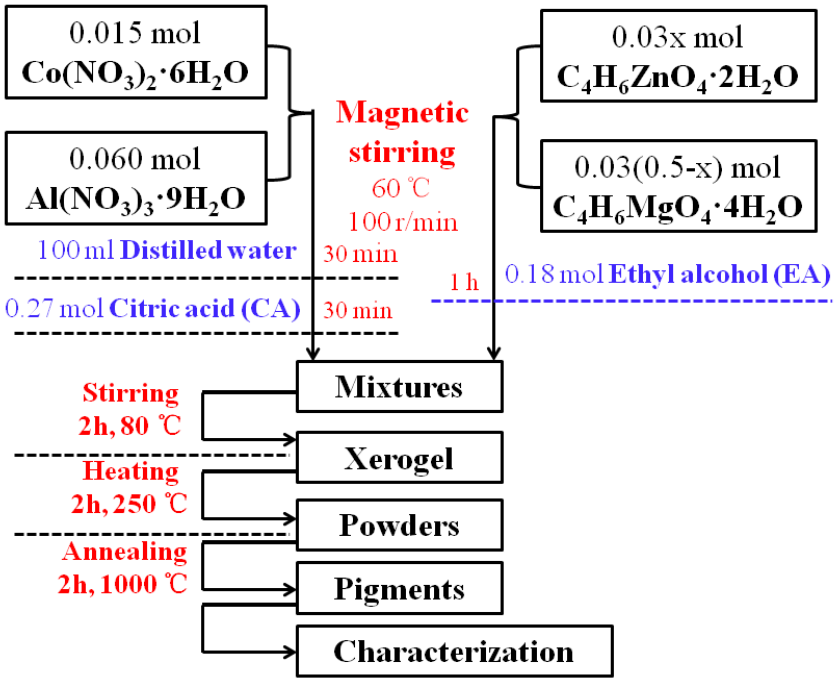

Fig. 1

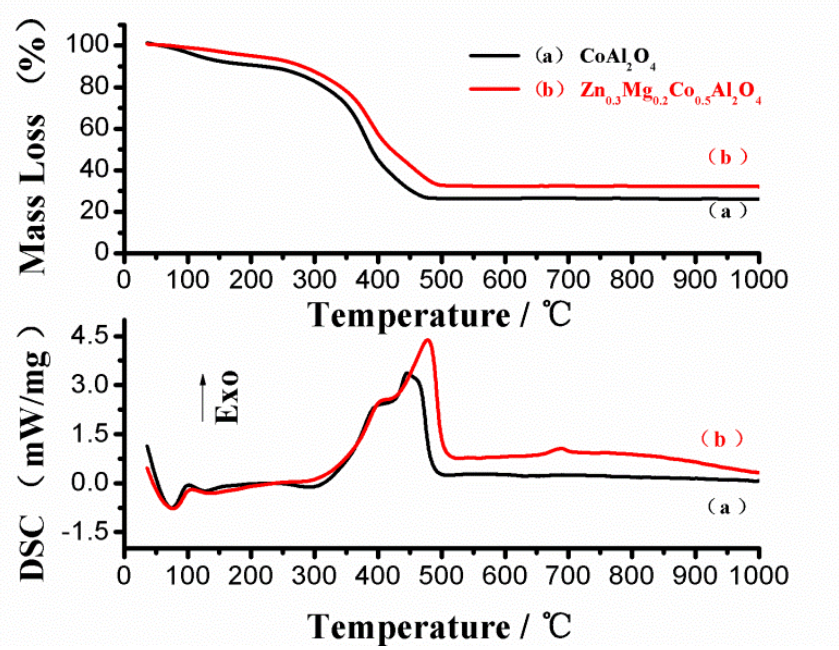

Fig. 2

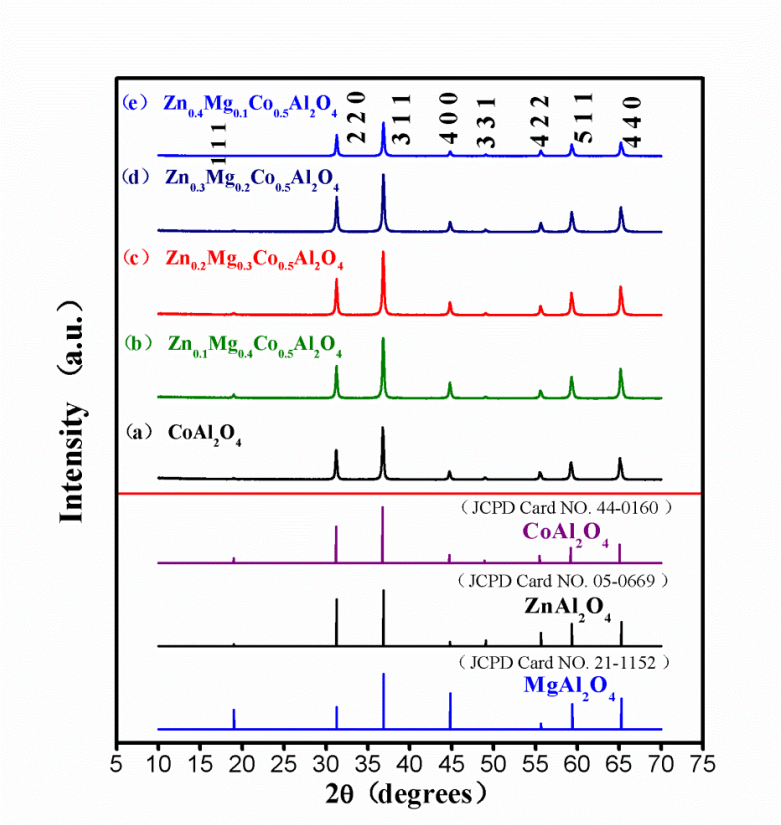
(e) Zn0.4Mg0.1Co0.5Al2O4
(d) Zn0.3Mg0.2Co0.5Al2O4
(c) Zn0.2Mg0.3Co0.5Al2O4
(b) Zn0.1Mg0.4Co0.5Al2O4
(a) CoAl2O4
111
220
311
400
331
422
511
440
Intensity (a.u.)
(JCPD Card NO. 44-0160)
CoAl2O4
(JCPD Card NO. 05-0669)
ZnAl2O4
(JCPD Card NO. 21-1152)
MgAl2O4
5 10 15 20 25 30 35 40 45 50 55 60 65 70 75
2θ (degrees)

Fig. 3

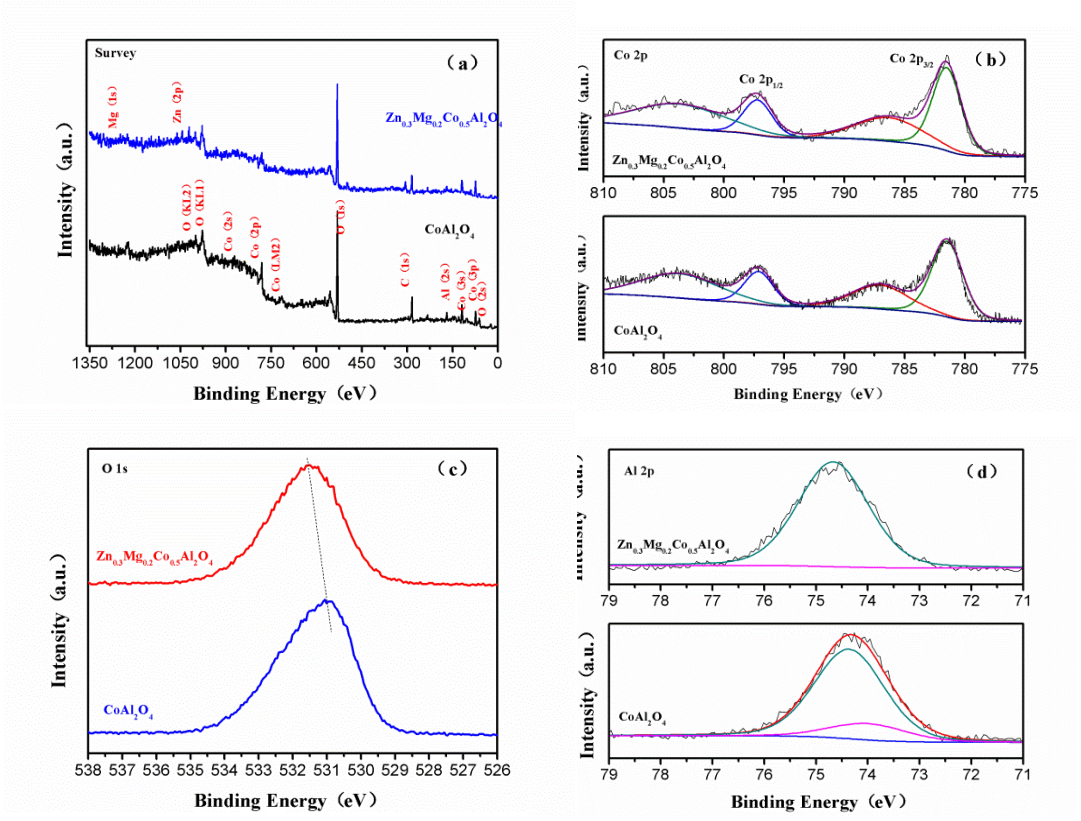
Survey
(a)
Mg (1s)
Zn (2p)
O (KL2)
O (KL1)
Co (2s)
Co (2p)
Co (LM2)
O (1s)
C (1s)
Al (2s)
Co (3s)
Co (3p)
O (2s)
Zn0.3Mg0.2Co0.5Al2O4
CoAl2O4
Intensity (a.u.)
1350 1200 1050 900 750 600 450 300 150 0
Binding Energy (eV)
Co 2p
(b)
Co 2p1/2
Co 2p3/2
Zn0.3Mg0.2Co0.5Al2O4
CoAl2O4
810 805 800 795 790 785 780 775
Binding Energy (eV)
O 1s
(c)
Zn0.3Mg0.2Co0.5Al2O4
CoAl2O4
538 537 536 535 534 533 532 531 530 529 528 527 526
Binding Energy (eV)
Al 2p
(d)
Zn0.3Mg0.2Co0.5Al2O4
CoAl2O4
79 78 77 76 75 74 73 72 71
Binding Energy (eV)

Fig. 4

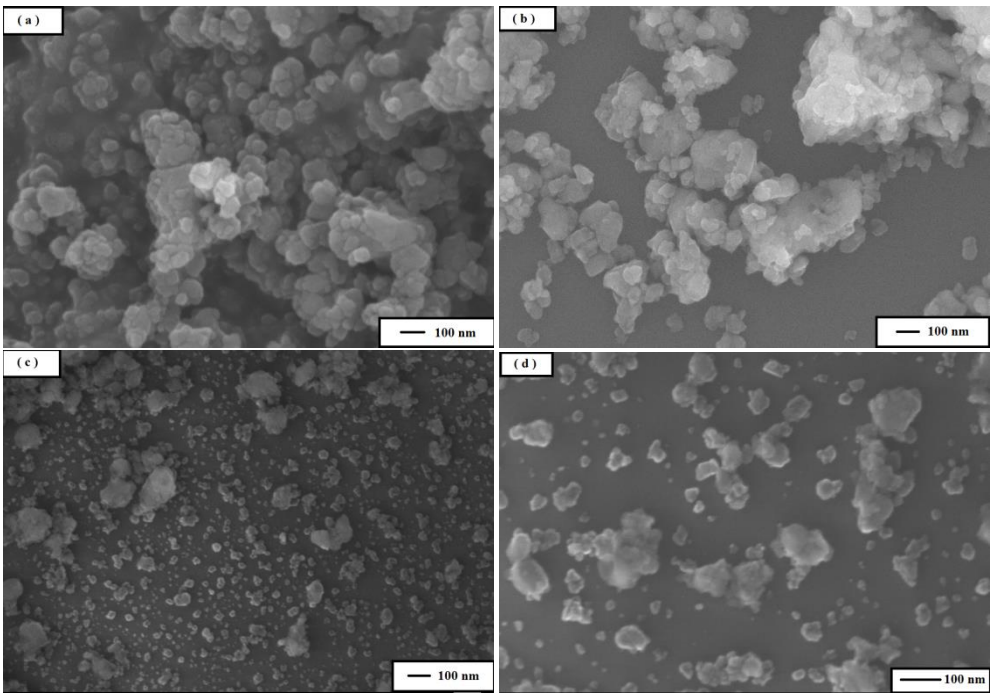
(a)
100 nm
(b)
100 nm
(c)
100 nm
(d)
100 nm

Fig. 5

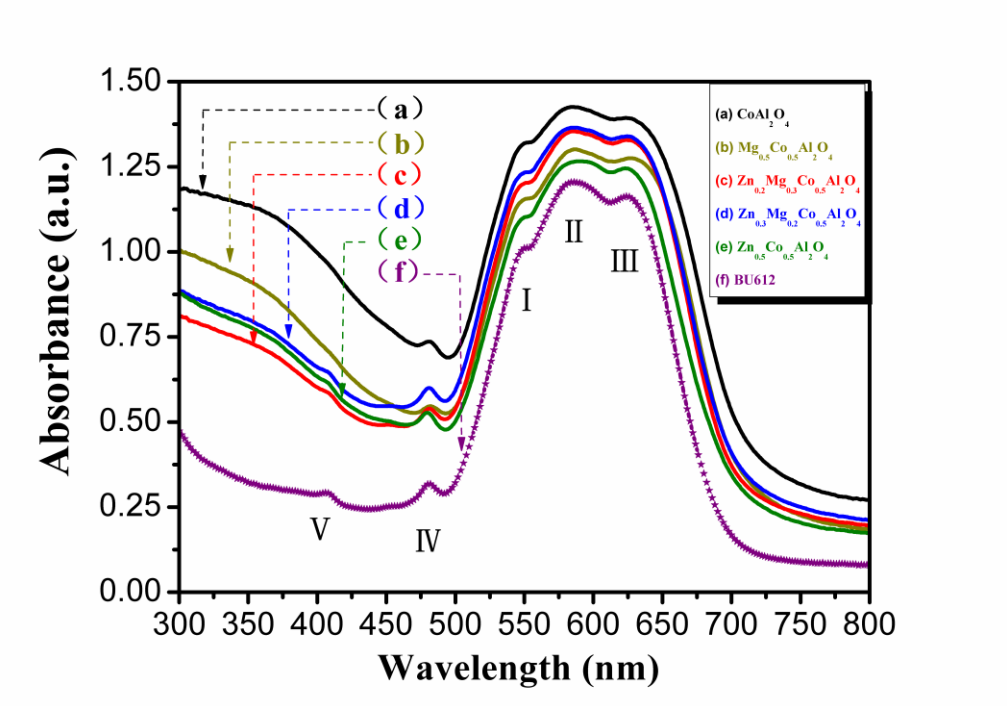
Absorbance (a.u.)
Wavelength (nm)
1.50
1.25
1.00
0.75
0.50
0.25
0.00
300 350 400 450 500 550 600 650 700 750 800
(a)
(b)
(c)
(d)
(e)
(f)
I
II
III
IV
V
(a) CoAl2O4
(b) Mg0.5Co0.5Al2O4
(c) Zn0.2Mg0.3Co0.5Al2O4
(d) Zn0.3Mg0.2Co0.5Al2O4
(e) Zn0.5Co0.5Al2O4
(f) BU612

Fig. 6

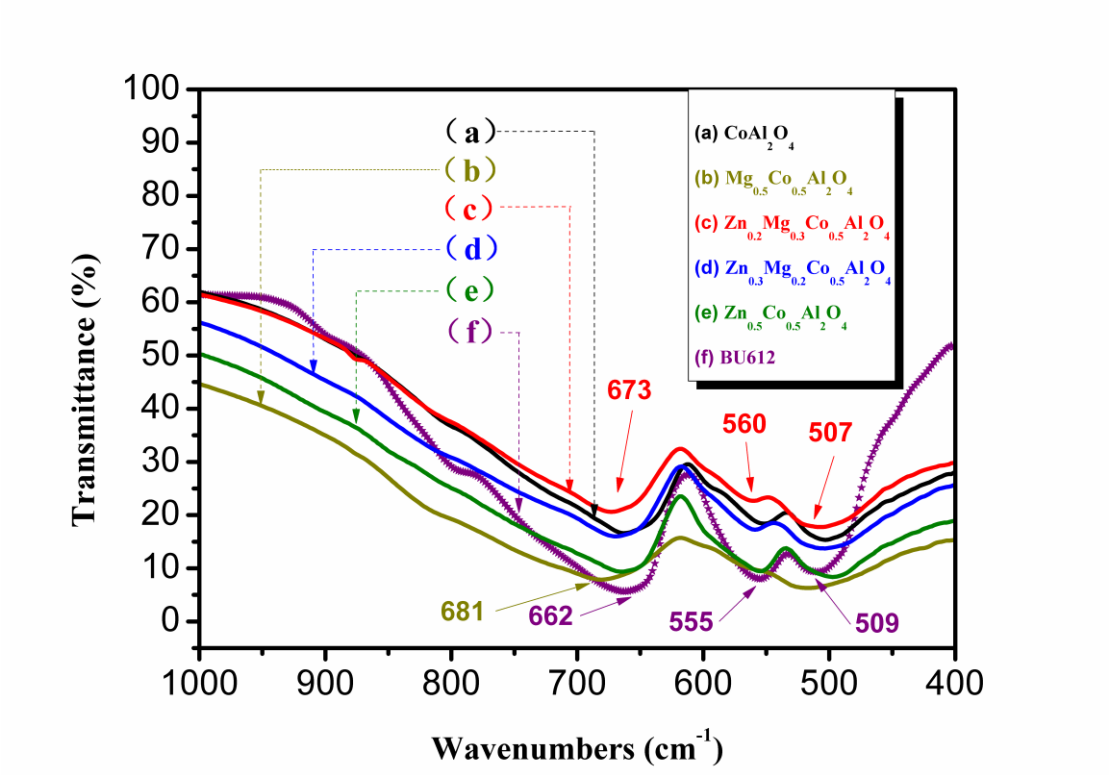
Transmittance (%)
Wavenumbers (cm-1)
(a)
(b)
(c)
(d)
(e)
(f)
(a) CoAl2O4
(b) Mg0.5Co0.5Al2O4
(c) Zn0.2Mg0.3Co0.5Al2O4
(d) Zn0.3Mg0.2Co0.5Al2O4
(e) Zn0.5Co0.5Al2O4
(f) BU612
673
560
507
681
662
555
509

Fig. 7

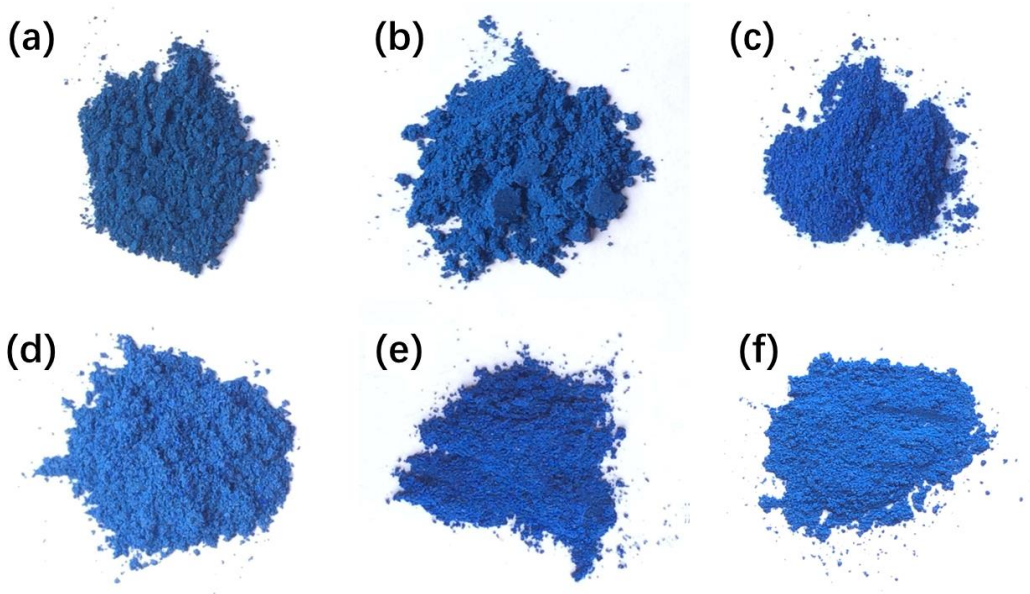
(a)
(b)
(c)
(d)
(e)
(f)

Fig. 8

Table captions：

Table 1 The particle size from XRD results and CIE-$L^*a^*b^*$ values of synthetic $CoAl_2O_4$ and $Zn_xMg_{0.5-x}Co_{0.5}Al_2O_4$ (x = 0, 0.1, 0.2, 0.3, 0.4, 0.5) solid solutions nanocrystals as well as commercial $CoAl_2O_4$ pigment (BU612).

Tables：

Table 1

	X	Y	$Zn_xMg_{1-x}Co_{0.5}Al_2O_4$	Crystallite size (± 0.5 nm)	L^*	a^*	b^*
ZM1			$CoAl_2O_4$	43	29.47	-12.44	-24.51
ZM2	0	0.5	$Mg_{0.5}Co_{0.5}Al_2O_4$	42	33.26	-9.6	-25.44
ZM3	0.1	0.4	$Zn_{0.1}Mg_{0.4}Co_{0.5}Al_2O_4$	40	33.75	-7.24	-26.57
ZM4	0.2	0.3	$Zn_{0.2}Mg_{0.3}Co_{0.5}Al_2O_4$	41	34.62	-8.31	-28.03
ZM5	0.3	0.2	$Zn_{0.3}Mg_{0.2}Co_{0.5}Al_2O_4$	39	35.82	-6.97	-28.27
ZM6	0.4	0.1	$Zn_{0.4}Mg_{0.1}Co_{0.5}Al_2O_4$	43	36.04	-7.35	-27.98
ZM7	0.5	0	$Zn_{0.5}Co_{0.5}Al_2O_4$	42	44.88	-8.49	-25.37
BU612			$CoAl_2O_4$		36.09	-11.25	-28.47

Environmental blue CoAl2O4 pigment co-doped by Zn2+ and Mg2+: synthesis, structure and optical properties

Peng, Xiaojin

2017-12-09

Peng X, Cheng J, Yuan J, Jin N, Kang J, Hou Y, Qi Z, Environmental blue CoAl2O4 pigment co-doped by Zn2+ and Mg2+: synthesis, structure and optical properties, Advances in Applied Ceramics, Volume 117, 2018, Issue 5, pp. 303-311

http://dx.doi.org/10.1080/17436753.2017.1410941